

Measurement of the $t\bar{t}$ Production Cross Section in $p\bar{p}$ Collisions at $\sqrt{s} = 1.96$ TeV using Kinematic Characteristics of Lepton + Jets Events

V.M. Abazov,³⁵ B. Abbott,⁷² M. Abolins,⁶³ B.S. Acharya,²⁹ M. Adams,⁵⁰ T. Adams,⁴⁸ M. Agelou,¹⁸ J.-L. Agram,¹⁹ S.H. Ahn,³¹ M. Ahsan,⁵⁷ G.D. Alexeev,³⁵ G. Alkhazov,³⁹ A. Alton,⁶² G. Alverson,⁶¹ G.A. Alves,² M. Anastasoae,³⁴ T. Andeen,⁵² S. Anderson,⁴⁴ B. Andrieu,¹⁷ Y. Arnaud,¹⁴ A. Askew,⁴⁸ B. Åsman,⁴⁰ A.C.S. Assis Jesus,³ O. Atramentov,⁵⁵ C. Autermann,²¹ C. Avila,⁸ F. Badaud,¹³ A. Baden,⁵⁹ B. Baldin,⁴⁹ P.W. Balm,³³ S. Banerjee,²⁹ E. Barberis,⁶¹ P. Bargassa,⁷⁶ P. Baringer,⁵⁶ C. Barnes,⁴² J. Barreto,² J.F. Bartlett,⁴⁹ U. Bassler,¹⁷ D. Bauer,⁵³ A. Bean,⁵⁶ S. Beauceron,¹⁷ M. Begel,⁶⁸ A. Bellavance,⁶⁵ S.B. Beri,²⁷ G. Bernardi,¹⁷ R. Bernhard,^{49,*} I. Bertram,⁴¹ M. Besançon,¹⁸ R. Beuselinck,⁴² V.A. Bezzubov,³⁸ P.C. Bhat,⁴⁹ V. Bhatnagar,²⁷ M. Binder,²⁵ C. Biscarat,⁴¹ K.M. Black,⁶⁰ I. Blackler,⁴² G. Blazey,⁵¹ F. Blekman,³³ S. Blessing,⁴⁸ D. Bloch,¹⁹ U. Blumenschein,²³ A. Boehnlein,⁴⁹ O. Boeriu,⁵⁴ T.A. Bolton,⁵⁷ F. Borchering,⁴⁹ G. Borissov,⁴¹ K. Bos,³³ T. Bose,⁶⁷ A. Brandt,⁷⁴ R. Brock,⁶³ G. Brooijmans,⁶⁷ A. Bross,⁴⁹ N.J. Buchanan,⁴⁸ D. Buchholz,⁵² M. Buehler,⁵⁰ V. Buescher,²³ S. Burdin,⁴⁹ T.H. Burnett,⁷⁸ E. Busato,¹⁷ C.P. Buszello,⁴² J.M. Butler,⁶⁰ J. Cammin,⁶⁸ S. Caron,³³ W. Carvalho,³ B.C.K. Casey,⁷³ N.M. Cason,⁵⁴ H. Castilla-Valdez,³² S. Chakrabarti,²⁹ D. Chakraborty,⁵¹ K.M. Chan,⁶⁸ A. Chandra,²⁹ D. Chapin,⁷³ F. Charles,¹⁹ E. Cheu,⁴⁴ D.K. Cho,⁶⁰ S. Choi,⁴⁷ B. Choudhary,²⁸ T. Christiansen,²⁵ L. Christofek,⁵⁶ D. Claes,⁶⁵ B. Clément,¹⁹ C. Clément,⁴⁰ Y. Coadou,⁵ M. Cooke,⁷⁶ W.E. Cooper,⁴⁹ D. Coppage,⁵⁶ M. Corcoran,⁷⁶ A. Cothenet,¹⁵ M.-C. Cousinou,¹⁵ B. Cox,⁴³ S. Crépe-Renaudin,¹⁴ D. Cutts,⁷³ H. da Motta,² B. Davies,⁴¹ G. Davies,⁴² G.A. Davis,⁵² K. De,⁷⁴ P. de Jong,³³ S.J. de Jong,³⁴ E. De La Cruz-Burelo,³² C. De Oliveira Martins,³ S. Dean,⁴³ J.D. Degenhardt,⁶² F. Déliot,¹⁸ M. Demarteau,⁴⁹ R. Demina,⁶⁸ P. Demine,¹⁸ D. Denisov,⁴⁹ S.P. Denisov,³⁸ S. Desai,⁶⁹ H.T. Diehl,⁴⁹ M. Diesburg,⁴⁹ M. Doidge,⁴¹ H. Dong,⁶⁹ S. Doulas,⁶¹ L.V. Dudko,³⁷ L. Dufflot,¹⁶ S.R. Dugad,²⁹ A. Duperrin,¹⁵ J. Dyer,⁶³ A. Dyshkant,⁵¹ M. Eads,⁵¹ D. Edmunds,⁶³ T. Edwards,⁴³ J. Ellison,⁴⁷ J. Elmsheuser,²⁵ V.D. Elvira,⁴⁹ S. Eno,⁵⁹ P. Ermolov,³⁷ O.V. Eroshin,³⁸ J. Estrada,⁴⁹ H. Evans,⁶⁷ A. Evdokimov,³⁶ V.N. Evdokimov,³⁸ J. Fast,⁴⁹ S.N. Fatakia,⁶⁰ L. Feligioni,⁶⁰ A.V. Ferapontov,³⁸ T. Ferbel,⁶⁸ F. Fiedler,²⁵ F. Filthaut,³⁴ W. Fisher,⁶⁶ H.E. Fisk,⁴⁹ I. Fleck,²³ M. Fortner,⁵¹ H. Fox,²³ S. Fu,⁴⁹ S. Fuess,⁴⁹ T. Gadfort,⁷⁸ C.F. Galea,³⁴ E. Gallas,⁴⁹ E. Galyaev,⁵⁴ C. Garcia,⁶⁸ A. Garcia-Bellido,⁷⁸ J. Gardner,⁵⁶ V. Gavrilov,³⁶ P. Gay,¹³ D. Gelé,¹⁹ R. Gelhaus,⁴⁷ K. Genser,⁴⁹ C.E. Gerber,⁵⁰ Y. Gershtein,⁴⁸ D. Gillberg,⁵ G. Ginter,⁶⁸ T. Golling,²² N. Gollub,⁴⁰ B. Gómez,⁸ K. Gounder,⁴⁹ A. Goussiou,⁵⁴ P.D. Grannis,⁶⁹ S. Greder,³ H. Greenlee,⁴⁹ Z.D. Greenwood,⁵⁸ E.M. Gregores,⁴ Ph. Gris,¹³ J.-F. Grivaz,¹⁶ L. Groer,⁶⁷ S. Grünendahl,⁴⁹ M.W. Grünewald,³⁰ S.N. Gurzhiev,³⁸ G. Gutierrez,⁴⁹ P. Gutierrez,⁷² A. Haas,⁶⁷ N.J. Hadley,⁵⁹ S. Hagopian,⁴⁸ I. Hall,⁷² R.E. Hall,⁴⁶ C. Han,⁶² L. Han,⁷ K. Hanagaki,⁴⁹ K. Harder,⁵⁷ A. Harel,²⁶ R. Harrington,⁶¹ J.M. Hauptman,⁵⁵ R. Hauser,⁶³ J. Hays,⁵² T. Hebbeker,²¹ D. Hedin,⁵¹ J.M. Heinmiller,⁵⁰ A.P. Heinson,⁴⁷ U. Heintz,⁶⁰ C. Hensel,⁵⁶ G. Hesketh,⁶¹ M.D. Hildreth,⁵⁴ R. Hirosky,⁷⁷ J.D. Hobbs,⁶⁹ B. Hoeneisen,¹² M. Hohlfield,²⁴ S.J. Hong,³¹ R. Hooper,⁷³ P. Houben,³³ Y. Hu,⁶⁹ J. Huang,⁵³ V. Hynek,⁹ I. Iashvili,⁴⁷ R. Illingworth,⁴⁹ A.S. Ito,⁴⁹ S. Jabeen,⁵⁶ M. Jaffré,¹⁶ S. Jain,⁷² V. Jain,⁷⁰ K. Jakobs,²³ A. Jenkins,⁴² R. Jesik,⁴² K. Johns,⁴⁴ M. Johnson,⁴⁹ A. Jonckheere,⁴⁹ P. Jonsson,⁴² A. Juste,⁴⁹ D. Käfer,²¹ M.M. Kado,⁴⁵ S. Kahn,⁷⁰ E. Kajfasz,¹⁵ A.M. Kalinin,³⁵ J. Kalk,⁶³ D. Karmanov,³⁷ J. Kasper,⁶⁰ D. Kau,⁴⁸ R. Kaur,²⁷ R. Kehoe,⁷⁵ S. Kermiche,¹⁵ S. Kesisoglou,⁷³ A. Khanov,⁶⁸ A. Kharchilava,⁵⁴ Y.M. Kharzheev,³⁵ H. Kim,⁷⁴ T.J. Kim,³¹ B. Klima,⁴⁹ M. Klute,²² J.M. Kohli,²⁷ M. Kopal,⁷² V.M. Korablev,³⁸ J. Kotcher,⁷⁰ B. Kothari,⁶⁷ A. Koubarovsky,³⁷ A.V. Kozelov,³⁸ J. Kozminski,⁶³ A. Kryemadhi,⁷⁷ S. Krzywdzinski,⁴⁹ Y. Kulik,⁴⁹ A. Kumar,²⁸ S. Kunori,⁵⁹ A. Kupco,¹¹ T. Kurča,²⁰ J. Kvita,⁹ S. Lager,⁴⁰ N. Lahrichi,¹⁸ G. Landsberg,⁷³ J. Lazoflores,⁴⁸ A.-C. Le Bihan,¹⁹ P. Lebrun,²⁰ W.M. Lee,⁴⁸ A. Leflat,³⁷ F. Lehner,^{49,*} C. Leonidopoulos,⁶⁷ J. Leveque,⁴⁴ P. Lewis,⁴² J. Li,⁷⁴ Q.Z. Li,⁴⁹ J.G.R. Lima,⁵¹ D. Lincoln,⁴⁹ S.L. Linn,⁴⁸ J. Linnemann,⁶³ V.V. Lipaev,³⁸ R. Lipton,⁴⁹ L. Lobo,⁴² A. Lobodenko,³⁹ M. Lokajicek,¹¹ A. Lounis,¹⁹ P. Love,⁴¹ H.J. Lubatti,⁷⁸ L. Lueking,⁴⁹ M. Lynker,⁵⁴ A.L. Lyon,⁴⁹ A.K.A. Maciel,⁵¹ R.J. Madaras,⁴⁵ P. Mättig,²⁶ C. Magass,²¹ A. Magerkurth,⁶² A.-M. Magnan,¹⁴ N. Makovec,¹⁶ P.K. Mal,²⁹ H.B. Malbouisson,³ S. Malik,⁵⁸ V.L. Malyshev,³⁵ H.S. Mao,⁶ Y. Maravin,⁴⁹ M. Martens,⁴⁹ S.E.K. Mattingly,⁷³ A.A. Mayorov,³⁸ R. McCarthy,⁶⁹ R. McCroskey,⁴⁴ D. Meder,²⁴ A. Melnitchouk,⁶⁴ A. Mendes,¹⁵ M. Merkin,³⁷ K.W. Merritt,⁴⁹ A. Meyer,²¹ J. Meyer,²² M. Michaut,¹⁸ H. Miettinen,⁷⁶ J. Mitrevski,⁶⁷ J. Molina,³ N.K. Mondal,²⁹ R.W. Moore,⁵ G.S. Muanza,²⁰ M. Mulders,⁴⁹ Y.D. Mutaf,⁶⁹ E. Nagy,¹⁵ M. Narain,⁶⁰ N.A. Naumann,³⁴ H.A. Neal,⁶² J.P. Negret,⁸ S. Nelson,⁴⁸ P. Neustroev,³⁹

C. Noeding,²³ A. Nomerotski,⁴⁹ S.F. Novaes,⁴ T. Nunnemann,²⁵ E. Nurse,⁴³ V. O'Dell,⁴⁹ D.C. O'Neil,⁵ V. Oguri,³ N. Oliveira,³ N. Oshima,⁴⁹ G.J. Otero y Garzón,⁵⁰ P. Padley,⁷⁶ N. Parashar,⁵⁸ S.K. Park,³¹ J. Parsons,⁶⁷ R. Partridge,⁷³ N. Parua,⁶⁹ A. Patwa,⁷⁰ G. Pawloski,⁷⁶ P.M. Perea,⁴⁷ E. Perez,¹⁸ P. Pétrouff,¹⁶ M. Petteni,⁴² L. Phaf,³³ R. Piegai,¹ M.-A. Pleier,⁶⁸ P.L.M. Podesta-Lerma,³² V.M. Podstavkov,⁴⁹ Y. Pogorelov,⁵⁴ A. Pomposh,⁷² B.G. Pope,⁶³ W.L. Prado da Silva,³ H.B. Prosper,⁴⁸ S. Protopopescu,⁷⁰ J. Qian,⁶² A. Quadt,²² B. Quinn,⁶⁴ K.J. Rani,²⁹ K. Ranjan,²⁸ P.A. Rapidis,⁴⁹ P.N. Ratoff,⁴¹ S. Reucroft,⁶¹ M. Rijssenbeek,⁶⁹ I. Ripp-Baudot,¹⁹ F. Rizatdinova,⁵⁷ S. Robinson,⁴² R.F. Rodrigues,³ C. Royon,¹⁸ P. Rubinov,⁴⁹ R. Ruchti,⁵⁴ V.I. Rud,³⁷ G. Sajot,¹⁴ A. Sánchez-Hernández,³² M.P. Sanders,⁵⁹ A. Santoro,³ G. Savage,⁴⁹ L. Sawyer,⁵⁸ T. Scanlon,⁴² D. Schaile,²⁵ R.D. Schamberger,⁶⁹ H. Schellman,⁵² P. Schieferdecker,²⁵ C. Schmitt,²⁶ C. Schwanenberger,²² A. Schwartzman,⁶⁶ R. Schwienhorst,⁶³ S. Sengupta,⁴⁸ H. Severini,⁷² E. Shabalina,⁵⁰ M. Shamim,⁵⁷ V. Shary,¹⁸ A.A. Shchukin,³⁸ W.D. Shephard,⁵⁴ R.K. Shivpuri,²⁸ D. Shpakov,⁶¹ R.A. Sidwell,⁵⁷ V. Simak,¹⁰ V. Sirotenko,⁴⁹ P. Skubic,⁷² P. Slattery,⁶⁸ R.P. Smith,⁴⁹ K. Smolek,¹⁰ G.R. Snow,⁶⁵ J. Snow,⁷¹ S. Snyder,⁷⁰ S. Söldner-Rembold,⁴³ X. Song,⁵¹ L. Sonnenschein,¹⁷ A. Sopczak,⁴¹ M. Sosebee,⁷⁴ K. Soustruznik,⁹ M. Souza,² B. Spurlock,⁷⁴ N.R. Stanton,⁵⁷ J. Stark,¹⁴ J. Steele,⁵⁸ K. Stevenson,⁵³ V. Stolin,³⁶ A. Stone,⁵⁰ D.A. Stoyanova,³⁸ J. Strandberg,⁴⁰ M.A. Strang,⁷⁴ M. Strauss,⁷² R. Ströhmer,²⁵ D. Strom,⁵² M. Strovink,⁴⁵ L. Stutte,⁴⁹ S. Sumowidagdo,⁴⁸ A. Sznajder,³ M. Talby,¹⁵ P. Tamburello,⁴⁴ W. Taylor,⁵ P. Telford,⁴³ J. Temple,⁴⁴ M. Tomoto,⁴⁹ T. Toole,⁵⁹ J. Torborg,⁵⁴ S. Towers,⁶⁹ T. Trefzger,²⁴ S. Trincaz-Duvoid,¹⁷ B. Tuchming,¹⁸ C. Tully,⁶⁶ A.S. Turcot,⁴³ P.M. Tuts,⁶⁷ L. Uvarov,³⁹ S. Uvarov,³⁹ S. Uzunyan,⁵¹ B. Vachon,⁵ R. Van Kooten,⁵³ W.M. van Leeuwen,³³ N. Varelas,⁵⁰ E.W. Varnes,⁴⁴ A. Vartapetian,⁷⁴ I.A. Vasilyev,³⁸ M. Vaupel,²⁶ P. Verdier,²⁰ L.S. Vertogradov,³⁵ M. Verzocchi,⁵⁹ F. Villeneuve-Seguiet,⁴² J.-R. Vlimant,¹⁷ E. Von Toerne,⁵⁷ M. Vreeswijk,³³ T. Vu Anh,¹⁶ H.D. Wahl,⁴⁸ L. Wang,⁵⁹ J. Warchol,⁵⁴ G. Watts,⁷⁸ M. Wayne,⁵⁴ M. Weber,⁴⁹ H. Weerts,⁶³ M. Wegner,²¹ N. Vermes,²² A. White,⁷⁴ V. White,⁴⁹ D. Wicke,⁴⁹ D.A. Wijngaarden,³⁴ G.W. Wilson,⁵⁶ S.J. Wimpenny,⁴⁷ J. Wittlin,⁶⁰ M. Wobisch,⁴⁹ J. Womersley,⁴⁹ D.R. Wood,⁶¹ T.R. Wyatt,⁴³ Q. Xu,⁶² N. Xuan,⁵⁴ S. Yacoob,⁵² R. Yamada,⁴⁹ M. Yan,⁵⁹ T. Yasuda,⁴⁹ Y.A. Yatsunenko,³⁵ Y. Yen,²⁶ K. Yip,⁷⁰ H.D. Yoo,⁷³ S.W. Youn,⁵² J. Yu,⁷⁴ A. Yurkewicz,⁶⁹ A. Zabi,¹⁶ A. Zatserklyaniy,⁵¹ M. Zdrazil,⁶⁹ C. Zeitnitz,²⁴ D. Zhang,⁴⁹ X. Zhang,⁷² T. Zhao,⁷⁸ Z. Zhao,⁶² B. Zhou,⁶² J. Zhu,⁶⁹ M. Zielinski,⁶⁸ D. Zieminska,⁵³ A. Zieminski,⁵³ R. Zitoun,⁶⁹ V. Zutshi,⁵¹ and E.G. Zverev³⁷

(DØ Collaboration)

¹ *Universidad de Buenos Aires, Buenos Aires, Argentina*

² *LAFEX, Centro Brasileiro de Pesquisas Físicas, Rio de Janeiro, Brazil*

³ *Universidade do Estado do Rio de Janeiro, Rio de Janeiro, Brazil*

⁴ *Instituto de Física Teórica, Universidade Estadual Paulista, São Paulo, Brazil*

⁵ *University of Alberta, Edmonton, Alberta, Canada, Simon Fraser University, Burnaby, British Columbia, Canada, York University, Toronto, Ontario, Canada, and McGill University, Montreal, Quebec, Canada*

⁶ *Institute of High Energy Physics, Beijing, People's Republic of China*

⁷ *University of Science and Technology of China, Hefei, People's Republic of China*

⁸ *Universidad de los Andes, Bogotá, Colombia*

⁹ *Center for Particle Physics, Charles University, Prague, Czech Republic*

¹⁰ *Czech Technical University, Prague, Czech Republic*

¹¹ *Institute of Physics, Academy of Sciences, Center for Particle Physics, Prague, Czech Republic*

¹² *Universidad San Francisco de Quito, Quito, Ecuador*

¹³ *Laboratoire de Physique Corpusculaire, IN2P3-CNRS, Université Blaise Pascal, Clermont-Ferrand, France*

¹⁴ *Laboratoire de Physique Subatomique et de Cosmologie, IN2P3-CNRS, Université de Grenoble 1, Grenoble, France*

¹⁵ *CPPM, IN2P3-CNRS, Université de la Méditerranée, Marseille, France*

¹⁶ *Laboratoire de l'Accélérateur Linéaire, IN2P3-CNRS, Orsay, France*

¹⁷ *LPNHE, IN2P3-CNRS, Universités Paris VI and VII, Paris, France*

¹⁸ *DAPNIA/Service de Physique des Particules, CEA, Saclay, France*

¹⁹ *IReS, IN2P3-CNRS, Université Louis Pasteur, Strasbourg, France, and Université de Haute Alsace, Mulhouse, France*

²⁰ *Institut de Physique Nucléaire de Lyon, IN2P3-CNRS, Université Claude Bernard, Villeurbanne, France*

²¹ *III. Physikalisches Institut A, RWTH Aachen, Aachen, Germany*

²² *Physikalisches Institut, Universität Bonn, Bonn, Germany*

²³ *Physikalisches Institut, Universität Freiburg, Freiburg, Germany*

²⁴ *Institut für Physik, Universität Mainz, Mainz, Germany*

²⁵ *Ludwig-Maximilians-Universität München, München, Germany*

²⁶ *Fachbereich Physik, University of Wuppertal, Wuppertal, Germany*

²⁷ *Panjab University, Chandigarh, India*

²⁸ *Delhi University, Delhi, India*

²⁹ *Tata Institute of Fundamental Research, Mumbai, India*

³⁰ *University College Dublin, Dublin, Ireland*

- ³¹*Korea Detector Laboratory, Korea University, Seoul, Korea*
³²*CINVESTAV, Mexico City, Mexico*
³³*FOM-Institute NIKHEF and University of Amsterdam/NIKHEF, Amsterdam, The Netherlands*
³⁴*Radboud University Nijmegen/NIKHEF, Nijmegen, The Netherlands*
³⁵*Joint Institute for Nuclear Research, Dubna, Russia*
³⁶*Institute for Theoretical and Experimental Physics, Moscow, Russia*
³⁷*Moscow State University, Moscow, Russia*
³⁸*Institute for High Energy Physics, Protvino, Russia*
³⁹*Petersburg Nuclear Physics Institute, St. Petersburg, Russia*
⁴⁰*Lund University, Lund, Sweden, Royal Institute of Technology and Stockholm University, Stockholm, Sweden, and Uppsala University, Uppsala, Sweden*
⁴¹*Lancaster University, Lancaster, United Kingdom*
⁴²*Imperial College, London, United Kingdom*
⁴³*University of Manchester, Manchester, United Kingdom*
⁴⁴*University of Arizona, Tucson, Arizona 85721, USA*
⁴⁵*Lawrence Berkeley National Laboratory and University of California, Berkeley, California 94720, USA*
⁴⁶*California State University, Fresno, California 93740, USA*
⁴⁷*University of California, Riverside, California 92521, USA*
⁴⁸*Florida State University, Tallahassee, Florida 32306, USA*
⁴⁹*Fermi National Accelerator Laboratory, Batavia, Illinois 60510, USA*
⁵⁰*University of Illinois at Chicago, Chicago, Illinois 60607, USA*
⁵¹*Northern Illinois University, DeKalb, Illinois 60115, USA*
⁵²*Northwestern University, Evanston, Illinois 60208, USA*
⁵³*Indiana University, Bloomington, Indiana 47405, USA*
⁵⁴*University of Notre Dame, Notre Dame, Indiana 46556, USA*
⁵⁵*Iowa State University, Ames, Iowa 50011, USA*
⁵⁶*University of Kansas, Lawrence, Kansas 66045, USA*
⁵⁷*Kansas State University, Manhattan, Kansas 66506, USA*
⁵⁸*Louisiana Tech University, Ruston, Louisiana 71272, USA*
⁵⁹*University of Maryland, College Park, Maryland 20742, USA*
⁶⁰*Boston University, Boston, Massachusetts 02215, USA*
⁶¹*Northeastern University, Boston, Massachusetts 02115, USA*
⁶²*University of Michigan, Ann Arbor, Michigan 48109, USA*
⁶³*Michigan State University, East Lansing, Michigan 48824, USA*
⁶⁴*University of Mississippi, University, Mississippi 38677, USA*
⁶⁵*University of Nebraska, Lincoln, Nebraska 68588, USA*
⁶⁶*Princeton University, Princeton, New Jersey 08544, USA*
⁶⁷*Columbia University, New York, New York 10027, USA*
⁶⁸*University of Rochester, Rochester, New York 14627, USA*
⁶⁹*State University of New York, Stony Brook, New York 11794, USA*
⁷⁰*Brookhaven National Laboratory, Upton, New York 11973, USA*
⁷¹*Langston University, Langston, Oklahoma 73050, USA*
⁷²*University of Oklahoma, Norman, Oklahoma 73019, USA*
⁷³*Brown University, Providence, Rhode Island 02912, USA*
⁷⁴*University of Texas, Arlington, Texas 76019, USA*
⁷⁵*Southern Methodist University, Dallas, Texas 75275, USA*
⁷⁶*Rice University, Houston, Texas 77005, USA*
⁷⁷*University of Virginia, Charlottesville, Virginia 22901, USA*
⁷⁸*University of Washington, Seattle, Washington 98195, USA*

(Dated: April 25, 2005)

We present a measurement of the top quark pair ($t\bar{t}$) production cross section ($\sigma_{t\bar{t}}$) in $p\bar{p}$ collisions at a center-of-mass energy of 1.96 TeV using 230 pb^{-1} of data collected by the DØ detector at the Fermilab Tevatron Collider. We select events with one charged lepton (electron or muon), large missing transverse energy, and at least four jets, and extract the $t\bar{t}$ content of the sample based on the kinematic characteristics of the events. For a top quark mass of 175 GeV, we measure $\sigma_{t\bar{t}} = 6.7_{-1.3}^{+1.4} \text{ (stat)}_{-1.1}^{+1.6} \text{ (syst)} \pm 0.4 \text{ (lumi)} \text{ pb}$, in good agreement with the standard model prediction.

PACS numbers: 13.85.Lg, 13.85.Qk, 14.65.Ha

Within the standard model (SM), top quarks are produced in $p\bar{p}$ collisions predominantly in pairs via the strong interaction ($q\bar{q}$ annihilation and gluon fusion), and decay almost exclusively to a W boson and a b

quark. The top quark pair production cross section $\sigma_{t\bar{t}}$ was measured by the CDF [1] and DØ [2] collaborations at a center-of-mass energy of 1.8 TeV. Recent measurements [3] of $\sigma_{t\bar{t}}$ at $\sqrt{s} = 1.96$ TeV have focused on the selection of candidates via the reconstruction of displaced vertices signaling the presence of b quarks in the final state. These measurements assume that the branching ratio of the top quark $B(t \rightarrow Wb) = 1$, thus making an implicit use of the SM prediction that $|V_{tb}| = 0.9990 \div 0.9992$ (at 90% C.L.) [4]. This prediction is based on the requirements that there are three fermion families and the CKM matrix is unitary. If these assumptions are relaxed, $|V_{tb}|$ is essentially unconstrained, which allows for large deviations of $B(t \rightarrow Wb)$ from unity [5]. Such deviations would be an indication of physics beyond the SM. Our analysis exploits only the kinematic properties of the events to separate signal from background, with no assumptions about the multiplicity of final-state b quarks, thus providing a less model-dependent determination of the top quark production cross section.

In this Letter, we report a new measurement of $\sigma_{t\bar{t}}$ using data collected with the DØ detector from August 2002 through March 2004 at the Fermilab Tevatron $p\bar{p}$ collider at $\sqrt{s} = 1.96$ TeV. The decay channel used in this analysis is $t\bar{t} \rightarrow W^+W^-q\bar{q}$, with the subsequent decay of one W boson into two quarks, and the other W boson into a charged lepton and a neutrino. We refer to this decay mode of $t\bar{t}$ events as the lepton+jets (ℓ +jets) channel. These events are characterized by the presence of one high- p_T isolated electron (e +jets channel) or muon (μ +jets channel), large transverse energy imbalance due to the undetected neutrino (\cancel{E}_T), and at least four hadronic jets.

The three main subsystems of the DØ Run II detector [6] used in this analysis are the central tracking system, the liquid-argon/uranium calorimeters, and the muon spectrometer. The central tracking system is located within a 2 Tesla superconducting solenoidal magnet, and consists of a silicon microstrip tracker (SMT) and a central fiber tracker (CFT) that provide tracking and vertexing in the pseudorapidity [7] range $|\eta| < 3.0$. The primary interaction vertex of the events was required to be within 60 cm of the center of the detector along the direction of the beam. Electrons and jets were detected in hermetic calorimeters [8, 9] with transverse granularity $\Delta\eta \times \Delta\phi = 0.1 \times 0.1$, where ϕ is the azimuthal angle. The third layer of the electromagnetic (EM) calorimeter, in which the maximum energy deposition of EM showers is expected, has a finer granularity $\Delta\eta \times \Delta\phi = 0.05 \times 0.05$. The calorimeters consist of a central section (CC) covering the region $|\eta| < 1.1$, and two end calorimeters (EC) extending coverage to $|\eta| \approx 4.2$. Muons were detected as tracks reconstructed from hits recorded in three layers of tracking detectors and two layers of scintillators [10], both located outside the calorimeter. A 1.8 Tesla iron toroidal magnet is located outside the innermost layer

of the muon detector. The luminosity was calculated by measuring the rate for $p\bar{p}$ inelastic collisions using two hodoscopes of scintillation counters mounted close to the beam pipe on the front surfaces of the EC calorimeters.

Jets were defined using a cone algorithm [11] with radius $\Delta\mathcal{R} = \sqrt{(\Delta\eta)^2 + (\Delta\phi)^2} = 0.5$. To improve calorimeter performance we use an algorithm that suppresses cells with negative energy as well as cells with energies significantly below the average electronics noise (unless they neighbor a cell of high positive energy). Identified jets were required to be confirmed by the independent trigger readout.

In the e +jets channel, we accepted electrons with $|\eta| < 1.1$ and jets with rapidity $|y| < 2.5$ [7]. At the trigger level, we required a single electron with transverse momentum (p_T) greater than 15 GeV, and a jet with $p_T > 15$ GeV (20 GeV) for the first (second) half of the data. The total integrated luminosity for this sample is 226 ± 15 pb $^{-1}$. The offline electron identification requirements consisted of the following: *i*) the electron had to deposit at least 90% of its energy in the electromagnetic calorimeter within a cone of radius $\Delta\mathcal{R} = 0.2$ relative to the shower axis; *ii*) the electron had to be isolated, i.e., the ratio of the energy in the hollow cone $0.2 < \Delta\mathcal{R} < 0.4$ to the reconstructed electron energy could not exceed 15%; *iii*) the transverse and longitudinal shower shapes had to be consistent with those expected for an electron (based on a detailed Monte Carlo simulation); and *iv*) a good spatial match had to exist between a reconstructed track in the tracking system and the shower position in the calorimeter. Electrons satisfying the above requirements are referred to as “loose.” For a “tight” electron, we required in addition, that a discriminant formed by combining the above variables with the information about impact parameter of the matched track relative to the primary interaction vertex, and the number and p_T of other tracks around the electron candidate, be consistent with the expectations for a high- p_T isolated electron.

In the μ +jets channel, we accepted muons with $|\eta| < 2.0$ and jets with $|y| < 2.5$. At the trigger level, we required a single muon detected outside the toroidal magnet (which corresponds to an effective minimum momentum of ≈ 3 GeV), and a jet with $p_T > 20$ GeV (25 GeV) for the first (second) half of the data. The total integrated luminosity for this sample is 229 ± 15 pb $^{-1}$. The offline muon identification requirements consisted of the following: *i*) a muon track segment on the inside of the toroid had to be matched to a muon track segment on the outside of the toroid; *ii*) the timing of the muon, based on information from associated scintillator hits, had to be inconsistent with that of a cosmic ray; *iii*) a track reconstructed in the tracking system and pointing to the event vertex was required to be matched to the muon candidate found in the muon system; *iv*) the reconstructed muon was required to be separated from

jets, $\Delta\mathcal{R}(\mu, \text{jet}) > 0.5$. Muons satisfying the above requirements are referred to as “loose.” For a “tight” muon we also applied a stricter isolation requirement based on the energy of calorimeter clusters and tracks around the muon candidate.

We selected 87 (80) events that had only one tight electron (muon) with $p_T > 20$ GeV, $\cancel{E}_T > 20$ GeV and not collinear with the lepton direction in the transverse plane, and at least four jets each with $p_T > 20$ GeV. We refer to these as the “tight” samples in the e +jets (μ +jets) channel. Removing the tight requirement on the lepton identification results in 230 (140) events passing the selection. We refer to these as the “loose” samples in the e +jets (μ +jets) channel.

Monte Carlo simulations of $t\bar{t}$ and W +jets events were used to calculate selection efficiencies and to simulate kinematic characteristics of the events. Top quark signal and W +jets background processes were generated at $\sqrt{s} = 1.96$ TeV using ALPGEN 1.2 [12] for the parton-level process, and PYTHIA 6.2 [13] for subsequent hadronization. Generated events were processed through the GEANT-based [14] DØ detector simulation and reconstructed with the same program used for collider data. Additional smearing was applied to the reconstructed objects to improve the agreement between data and simulation. Remaining discrepancies in the description of the object reconstruction and identification between the simulation and the data were taken into account with correction factors derived by comparing the efficiencies measured in $Z \rightarrow \ell^+\ell^-$ data events to the ones obtained from the simulation. Lepton and jet trigger efficiencies derived from data were also applied to the simulated events. The fully corrected efficiencies to select $t\bar{t}$ events were found to be $(11.6 \pm 1.7)\%$ and $(11.7 \pm 1.9)\%$ in the e +jets and μ +jets channel, respectively. These efficiencies are calculated with respect to all $t\bar{t}$ final states that contain an electron or a muon originating either directly from a W boson or indirectly from $W \rightarrow \tau\nu$ decay. The branching fractions of such final states are 17.106% and 17.036% [4] for the e +jets and μ +jets channels, respectively.

The background within the selected samples is dominated by W +jets events, which have the same signature as $t\bar{t}$ signal events. The samples also include contributions from multijet events in which a jet is misidentified as an electron (e +jets channel) or in which a muon originating from the semileptonic decay of a heavy quark appears isolated (μ +jets channel). In addition, significant \cancel{E}_T can arise from fluctuations and mismeasurements of the jet energies. We call these instrumental backgrounds “multijet background” and we estimated their contribution directly from data, following the “matrix” method described in Ref. [15] with the loose and tight samples described above. The loose sample consists of N_s signal events and N_b multijet background events, where N_s is a combination of W +jets and $t\bar{t}$ events. The tight sample consists of $\varepsilon_s N_s$ signal events and $\varepsilon_b N_b$ multijet back-

ground events, where ε_s and ε_b are the lepton selection efficiencies for the tight sample relative to the loose sample, for signal and background, respectively. We measured ε_s from a combination of $t\bar{t}$ and W +4 jets simulated events, and applied a correction factor derived from the comparison of the corresponding efficiency in the $Z \rightarrow \ell^+\ell^-$ data and simulation. We obtained ε_b from events with $\cancel{E}_T < 10$ GeV, which are dominated by multijet background; ε_b was found to be independent of jet multiplicity. For the e +jets channel, $\varepsilon_s = 0.82 \pm 0.02$, and $\varepsilon_b = 0.16 \pm 0.04$. For the μ +jets channel, $\varepsilon_s = 0.81 \pm 0.02$, and $\varepsilon_b = 0.09 \pm 0.03$.

To extract the fraction of $t\bar{t}$ events in the sample we constructed a discriminant function that makes use of the differences between the kinematic properties of the $t\bar{t}$ events and the W +jets background. We did not need to consider the multijet background separately from the W +jets background because the kinematic properties of these two event types are similar. We selected the set of variables that provide the best separation between signal and background, but have the least sensitivity to the dominant systematic uncertainties coming from the jet energy calibration and the W +jets background model. To reduce the dependence on modeling of soft radiation and underlying event, only the four highest p_T jets were used to determine these variables. The optimal discriminant function was found to be built from six variables: *i*) H_T , the scalar sum of the p_T of the four leading jets; *ii*) $\Delta\phi(\ell, \cancel{E}_T)$, the azimuthal opening angle between the lepton and the missing transverse energy; *iii*) $K_{T\min} = \Delta R_{jj}^{\min} p_T^{\min} / E_T^W$, where ΔR_{jj}^{\min} is the minimum separation in $\eta - \phi$ space between pairs of jets, p_T^{\min} is the p_T of the lower- p_T jet of that pair, and E_T^W is a scalar sum of the lepton transverse momentum and \cancel{E}_T ; *iv*) the event centrality \mathcal{C} , defined as the ratio of the scalar sum of the p_T of the jets to the scalar sum of the energy of the jets; *v*) the event aplanarity \mathcal{A} , constructed from the four-momenta of the lepton and the jets; and *vi*) the event sphericity \mathcal{S} , constructed from the four-momenta of the jets. The last two variables characterize the event shape and are defined, for example, in Ref. [16].

The discriminant function was built using the method described in Ref. [17], and has the following general form:

$$\mathcal{D} = \frac{S(x_1, x_2, \dots)}{S(x_1, x_2, \dots) + B(x_1, x_2, \dots)}, \quad (1)$$

where x_1, x_2, \dots is a set of input variables and $S(x_1, x_2, \dots)$ and $B(x_1, x_2, \dots)$ are the probability density functions for the $t\bar{t}$ signal and background, respectively. Neglecting the correlations between the input variables, the discriminant function can be approximated by the expression:

$$\mathcal{D} = \frac{\prod_i s_i(x_i)/b_i(x_i)}{\prod_i s_i(x_i)/b_i(x_i) + 1}, \quad (2)$$

where $s_i(x_i)$ and $b_i(x_i)$ are the normalized distributions of variable i for signal and background, respectively. As

constructed, the discriminant function peaks near zero for the background, and near unity for the signal. We modeled it using simulated $t\bar{t}$ and W +jets events, and a data sample selected by requiring that the leptons fail the tight selection criterion, representative of the multijet background. A Poisson maximum-likelihood fit of the modeled discriminant function distribution to that of the data yielded the top quark cross section $\sigma_{t\bar{t}}$ and the numbers of W +jets and multijet background events in the selected data sample. The multijet background was constrained within errors to the level determined by the matrix method.

Figure 1 shows the distribution of the discriminant function for data along with the fitted contributions from $t\bar{t}$ signal, W +jets, and multijet background events. The kinematic distributions observed in lepton+jets events are well described by the sum of $t\bar{t}$ signal, W +jets, and multijet background contributions. An example of this agreement is illustrated in Fig. 2 for events selected requiring $\mathcal{D} < 0.5$, dominated by background, and events in the $t\bar{t}$ signal region of $\mathcal{D} > 0.5$, for a variable that is not included in the discriminant function, namely, the highest jet p_T in the event.

The measurement of the $t\bar{t}$ production cross section at $\sqrt{s} = 1.96$ TeV in each lepton channel separately yields:

$$\begin{aligned} e + \text{jets} : \sigma_{t\bar{t}} &= 8.2_{-1.9}^{+2.1} (\text{stat}) {}_{-1.3}^{+1.9} (\text{syst}) \pm 0.5 (\text{lumi}) \text{ pb}, \\ \mu + \text{jets} : \sigma_{t\bar{t}} &= 5.4_{-1.6}^{+1.8} (\text{stat}) {}_{-1.0}^{+1.2} (\text{syst}) \pm 0.4 (\text{lumi}) \text{ pb}, \end{aligned}$$

assuming a top quark mass (m_t) of 175 GeV. These results agree within statistical uncertainties.

The combined cross section was estimated by minimizing the sum of the negative log-likelihood functions for each individual channel yielding

$$\sigma_{t\bar{t}} = 6.7_{-1.3}^{+1.4} (\text{stat}) {}_{-1.1}^{+1.6} (\text{syst}) \pm 0.4 (\text{lumi}) \text{ pb}$$

for $m_t = 175$ GeV. We treated systematic uncertainties contributing to the error on the event selection efficiency and the likelihood fit as fully correlated between each other and between the channels. The contributions to the systematic uncertainty from the different sources considered in the analysis are presented in Table I. The jet energy calibration uncertainty dominates, and represents about 90% of the total systematic uncertainty on the cross section. In addition, a systematic uncertainty of 6.5% from the luminosity measurement [18] has been assigned. In the top quark mass range of 160 GeV to 190 GeV, the measured cross section decreases (increases) by 0.11 pb per 1 GeV shift of m_t above (below) 175 GeV.

In summary, we have measured the top quark pair production cross section in $p\bar{p}$ collisions at $\sqrt{s} = 1.96$ TeV in the lepton+jets channel. Our measurement is consistent with the SM expectation [19] which predicts a cross section of 6.77 ± 0.42 pb for a top quark mass of 175 GeV.

We thank the staffs at Fermilab and collaborating institutions, and acknowledge support from the DOE and

TABLE I: Summary of systematic uncertainties $\Delta\sigma_{t\bar{t}}$ (pb).

Source	e +jets	μ +jets	ℓ +jets
Lepton identification	± 0.3	± 0.2	± 0.2
Jet energy calibration	$+ 1.8 - 1.2$	$+ 1.0 - 0.7$	$+ 1.4 - 1.0$
Jet identification	$+ 0.2 - 0.2$	$+ 0.2 - 0.1$	$+ 0.2 - 0.1$
Trigger	$+ 0.1 - 0.1$	$+ 0.4 - 0.3$	$+ 0.3 - 0.2$
Multijet background	± 0.3	± 0.03	± 0.2
W background model	± 0.2	± 0.4	± 0.3
MC statistics	± 0.5	± 0.3	± 0.3
Other	± 0.2	± 0.1	± 0.2
Total	$+ 1.9 - 1.3$	$+ 1.2 - 1.0$	$+ 1.6 - 1.1$

NSF (USA), CEA and CNRS/IN2P3 (France), FASI, Rosatom and RFBR (Russia), CAPES, CNPq, FAPERJ, FAPESP and FUNDUNESP (Brazil), DAE and DST (India), Colciencias (Colombia), CONACyT (Mexico), KRF (Korea), CONICET and UBACyT (Argentina), FOM (The Netherlands), PPARC (United Kingdom), MSMT (Czech Republic), CRC Program, CFI, NSERC and WestGrid Project (Canada), BMBF and DFG (Germany), SFI (Ireland), A.P. Sloan Foundation, Research Corporation, Texas Advanced Research Program, Alexander von Humboldt Foundation, and the Marie Curie Fellowships.

[*] Visitor from University of Zurich, Zurich, Switzerland.

- [1] CDF Collaboration, T. Affolder *et al.*, Phys. Rev. D **64**, 032002 (2001).
- [2] DØ Collaboration, V. Abazov *et al.*, Phys. Rev. D **67**, 012004 (2003).
- [3] CDF Collaboration, D. Acosta *et al.*, Phys. Rev. D **71**, 072005 (2005); CDF Collaboration, D. Acosta *et al.*, Phys. Rev. D **71**, 052003 (2005).
- [4] S. Eidelman *et al.*, Phys. Lett. B **592**, 1 (2004).
- [5] CDF Collaboration, T. Affolder *et al.*, Phys. Rev. Lett. **86**, 3233 (2001).
- [6] DØ Collaboration, V. Abazov *et al.*, “The Upgraded DØ Detector,” in preparation for submission to Nucl. Instrum. Meth. Phys. Res. A.
- [7] Rapidity y and pseudorapidity η are defined as functions of the polar angle θ as $y(\theta, \beta) \equiv \frac{1}{2} \ln [(1 + \beta \cos \theta)/(1 - \beta \cos \theta)]$; $\eta(\theta) \equiv y(\theta, 1)$, where β is a ratio of particle momentum to its energy.
- [8] H. Aihara *et al.*, Nucl. Instr. Meth. A **325**, 393 (1993).
- [9] S. Abachi *et al.*, Nucl. Instr. Meth. A **324**, 53 (1993).
- [10] V. Abazov *et al.*, Fermilab-PUB-05-034-E.
- [11] We are using the iterative, seed-based cone algorithm including midpoints, as described on p. 47 in G. C. Blazey *et al.*, in Proceedings of the Workshop: “QCD and Weak Boson Physics in Run II,” edited by U. Baur, R. K. Ellis, and D. Zeppenfeld, Fermilab-Pub-00/297 (2000).
- [12] M.L. Mangano *et al.*, JHEP **07**, 001 (2003).
- [13] T. Sjöstrand *et al.*, Comp. Phys. Commun. **135**, 238 (2001).
- [14] R. Brun and F. Carminati, CERN program library long

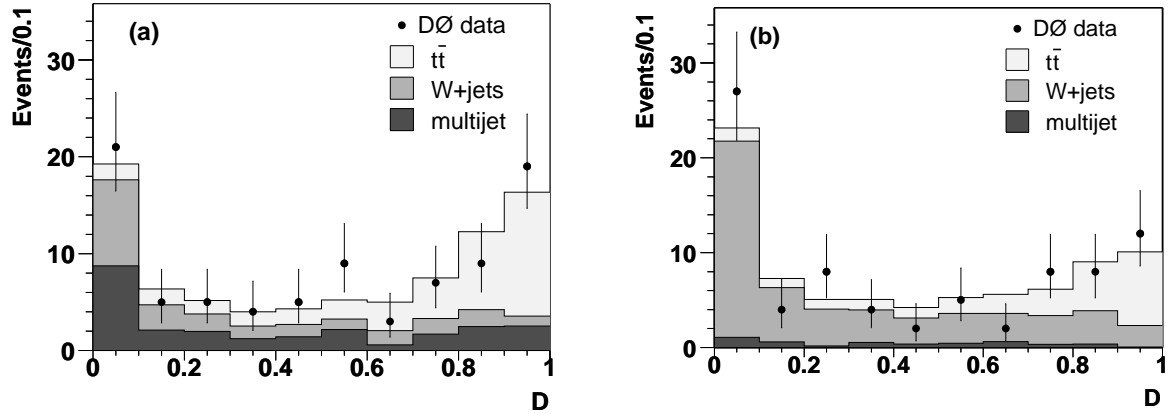


FIG. 1: Discriminant distribution for data overlaid with the result from a fit of $t\bar{t}$ signal, and $W+jets$ and multijet background (a) in the $e+jets$ channel and (b) in the $\mu+jets$ channel.

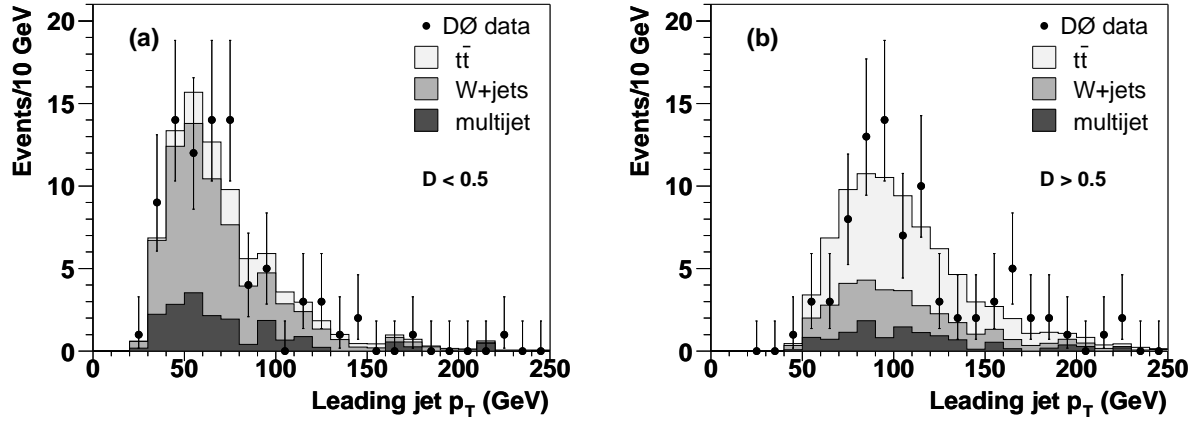


FIG. 2: Leading jet p_T distribution for $\ell+jets$ events in data with (a) discriminant below 0.5 and (b) discriminant above 0.5, overlaid with the result from a fit of $t\bar{t}$ signal, and $W+jets$ and multijet background.

writeup W5013 (1993).

- [15] DØ Collaboration, B. Abbott *et al.*, Phys. Rev. D **61**, 072001 (2000).
 [16] V. Barger, J. Ohnemus, and R.J.N. Phillips, Phys. Rev. D **48**, 3953 (1993).
 [17] DØ Collaboration, B. Abbott *et al.*, Phys. Rev. D **58**,

052001 (1998).

- [18] T. Edwards *et al.*, FERMILAB-TM-2278-E (2004).
 [19] R. Bonciani *et al.*, Nucl. Phys. B **529**, 424 (1998); N. Kidonakis and R. Vogt, Phys. Rev. D **68**, 114014 (2003); M. Cacciari *et al.*, JHEP **404**, 68 (2004).